Developmental Biology 356 (2011) 51–62

Contents lists available at ScienceDirect

Developmental Biology

journal homepage: www.elsevier.com/developmentalbiology

The E3 ubiquitin ligase Cullin 4A regulates meiotic progression in mouse spermatogenesis

Yan Yin [a], Congxing Lin [a], Sung Tae Kim [b], Ignasi Roig [c,d], Hong Chen [a], Liren Liu [e], George Michael Veith [a], Ramon U. Jin [f], Scott Keeney [c,g], Maria Jasin [h], Kelle Moley [i], Pengbo Zhou [e], Liang Ma [a,*]

[a] Division of Dermatology, Washington University School of Medicine, St. Louis, MO, USA
[b] Renal Division, Washington University School of Medicine, St. Louis, MO, USA
[c] Molecular Biology Program, Memorial Sloan-Kettering Cancer Center, New York, NY, USA
[d] Cytology and Histology Unit, Department of Cell Biology, Physiology & Immunology, Universitat Autònoma de Barcelona, Spain
[e] Department of Pathology and Laboratory Medicine, Weill Medical College and Graduate School of Medical Sciences of Cornell University, New York, NY, USA
[f] Division of Gastroenterology, Department of Medicine, Washington University School of Medicine, St. Louis, MO, USA
[g] Howard Hughes Medical Institute, Memorial Sloan-Kettering Cancer Center, 1275 York Avenue, New York, NY 10065, USA
[h] Developmental Biology, Memorial Sloan-Kettering Cancer Center, New York, NY, USA
[i] Department of Obstetrics and Gynecology, Washington University School of Medicine, St. Louis, MO, USA

ARTICLE INFO

Article history:
Received for publication 4 February 2011
Revised 12 May 2011
Accepted 13 May 2011
Available online 23 May 2011

Keywords:
Meiosis
Mlh1
Cullin4

ABSTRACT

The Cullin-RING ubiquitin-ligase CRL4 controls cell cycle and DNA damage checkpoint response and ensures genomic integrity. Inactivation of the *Cul4* component of the CRL4 E3 ligase complex in *Caenorhabditis elegans* by RNA interference results in massive mitotic DNA re-replication in the blast cells, largely due to failed degradation of the DNA licensing protein, CDT-1, and premature spermatogenesis. Here we show that inactivation of *Cul4a* by gene-targeting in mice only affected male but not female fertility. This male infertility phenotype resulted from a combination of decreased spermatozoa number, reduced sperm motility and defective acrosome formation. Agenesis of the mutant germ cells was accompanied by increased cell death in pachytene/diplotene cells with markedly elevated levels of phospho-p53 and CDT-1. Despite apparent normal assembly of synaptonemal complexes and DNA double strand break repair, dissociation of MLH1, a component of the late recombination nodule, was delayed in *Cul4a*−/− diplotene spermatocytes, which potentially led to subsequent disruptions in meiosis II and spermiogenesis. Together, our study revealed an indispensable role for *Cul4a* during male germ cell meiosis.

Introduction

Male infertility, a major issue in reproduction, affects approximately one in 25 men in the US (Schiff et al., 2007). Although its etiology is heterogeneous, it is usually associated with oligozoospermia (low sperm count), poor sperm motility and abnormal sperm morphology. Mammalian spermatogenesis is a complex and highly orchestrated process which transforms pluripotent spermatogonia into mature male gametes, the spermatozoa. In the seminiferous tubules of the testis, pluripotent A spermatogonia undergo several rounds of mitosis before differentiating into B spermatogonia. B spermatogonia then give rise to pre-leptotene primary spermatocytes which mark entry into meiosis I. Primary spermatocytes spend up to several weeks in meiosis I prophase and progress through leptotene, zygotene, pachytene and diplotene stages to prepare for cell division at metaphase I, as they physically move in toward the tubule lumen. After diakinesis, secondary spermatocytes rapidly go through meiosis II and become round spermatids. These cells undergo spermiogenesis to differentiate into spermatozoa. Defects that occur in any of these steps can lead to compromised male fertility.

The majority of such defects happen in prophase I, when homologous recombination occurs. During prophase I, chromosomes condense (leptotene) and pair up (zygotene) and the synaptonemal complex assembles along homologous chromosomes where recombination takes place (pachytene). The synaptonemal complex subsequently disassembles (diplotene) and DNA further condenses (diakinesis) before the first meiotic division (metaphase I). The progression of prophase I is regulated by many factors including those involved in DNA repair, homologous recombination as well as structural proteins. In the mouse, for example, deficiency in SPO11, a topoisomerase-like transesterase that initiates recombination by introducing double strand breaks (DSBs), causes failure of germ cells to proceed to the pachytene stage and leads to subsequent apoptosis of those cells (Baudat et al., 2000), while mutation in *Msh4*, a DNA mismatch repair gene, results in arrest of spermatocytes at the zygotene stage (Kneitz et al., 2000).

* Corresponding author at: Department of Medicine, Box 8123, Washington University, 660 S. Euclid Ave., St. Louis, MO 63110, USA. Fax: +1 314 454 5626.
E-mail address: lima@dom.wustl.edu (L. Ma).

0012-1606/$ – see front matter © 2011 Elsevier Inc. All rights reserved.
doi:10.1016/j.ydbio.2011.05.661

Ubiquitin-dependent proteolysis is essential for virtually all steps of mammalian spermatogenesis (Sutovsky, 2003). Many key regulatory proteins are targeted by this machinery early in mitosis and meiosis of germ cells. In addition, rapid degradation of cytoplasmic as well as nuclear proteins during spermiogenesis also relies on this machinery. Ubiquitination involves orchestrated actions of ubiquitin-activating, conjugating and ligating enzymes (Pickart, 2001). The Cullin gene family is the largest ubiquitin ligase family in mammals. Cullin 4A (CUL4A), one of the seven vertebrate Cullin proteins, binds to the RING finger protein Rbx1/ROC1/Hrt1 at its C-terminus for E2 conjugating enzyme recruitment, and to the damaged DNA binding protein 1 (DDB1) adaptor protein at the N-terminus for substrate recruitment. Together, this protein complex is referred to as CRL4. Proteins DDB1, and CUL4A-associated factors (DCAFs) function as substrate receptors in this process which brings substrates to the CRL4 complex for ubiquitination. In simpler organisms such as *Drosophila melanogaster* and *Caenorhabditis elegans*, there is only one *Cul4* gene. *Cul4* silencing by RNAi in *C. elegans* results in DNA re-replication in blast cells, and male germ cells undergo premature spermatogenesis (Zhong et al., 2003). In mammals, the CUL4 family has another member, CUL4B, which shares 89% sequence homology and some functional redundancy with CUL4A (Higa et al., 2003; Hu et al., 2004; Liu et al., 2009). We recently reported that germline-deletion of *Cul4a* in mice did not affect development, growth and viability of the animals, likely due to functional compensation from *Cul4b*. Nonetheless, epidermal-specific removal of *Cul4a* significantly enhanced nucleotide excision repair and G1/S DNA damage checkpoint pathways, rendering mutant animals hyper-resistant to UVB-induced skin carcinogenesis (Liu et al., 2009). In the current study, we explored *Cul4a* functions in murine spermatogenesis and showed that germline-deletion of *Cul4a* led to male infertility. Primary *Cul4a*−/− spermatocytes accumulated at the pachytene/diplotene stage, some underwent massive cell death and the rest produced malformed spermatozoa. These results demonstrated a critical role for *Cul4a* in mediating meiotic progression in spermatogenesis.

Materials and methods

Mice

Generation of *Cul4a*$^{c/c}$ animals was described previously (Liu et al., 2009). *EIIa*Cre and *Prm*-Cre transgenic mice were purchased from the Jackson Laboratory (Bar Harbor, Maine). All mice were housed in a barrier facility at Washington University in St. Louis and all animal experiments were performed in accordance to the institution's regulations with an approved protocol.

Histology, TUNEL and immunofluorescence (IF) of testicular tissue

Fresh testes were fixed in 4% paraformaldehyde (PFA) or Bouin's fixative, embedded and sectioned at 6 μm. Bouin-fixed sections were used for hematoxylin and eosin (H&E) staining and immunofluorescence (IF), and PFA-fixed sections were used for terminal deoxynucleotidyl transferase-mediated deoxyuridine triphosphate nick end labeling (TUNEL) staining, as described previously (Yin et al., 2006). For TUNEL-IF double-labeling, normal IF was performed first. After secondary antibody incubation, enzyme mix for TUNEL (Roche Applied Sciences) was applied and incubated for an hour. Slides were then washed and subsequently counter-stained with the Hoechst 33258 dye. Antibodies and dilutions used are: 1:100 for CUL4A (Bethyl Laboratories, Montgomery, TX), CUL4B (Proteintech Group, Chicago, IL), PLZF (CalBiochem, Gibbstown, NJ) and DDB1 (Bethyl Laboratories); 1:200 for PCNA (Cell Signalling Technology, Danvers, MA); 1:50 for GATA-1 (Santa Cruz Biotechnology, Santa Cruz, CA); 1:1000 for Alexa594 goat anti-rabbit, Alexa488 goat anti-mouse and Alexa594 goat anti-rat secondary antibodies (Invitrogen, Carlsbad, CA).

Sperm spread preparation, staining and histology

Cauda epididymides from males 2–6 months of age and their littermate controls were removed and put in warm DMEM. Tissues were punctuated with a 25-gage needle and incubated at 37 °C to allow sperms to swim out. To make sperm spread, aliquots of the medium were pipetted onto glass slides and smeared. Slides were dried and processed for routine H&E staining. To stain sperms with MitoTracker and PNA lectin, aliquots of sperm solution were transferred to microcentrifuge tubes and sperms were collected by centrifugation at 500×*g*. Live sperms were incubated with MitoTracker solution (Invitrogen) at 37 °C for 15 min. Sperms were then collected by centrifugation, fixed in 4% PFA, permeabilized in 0.2% Triton-X 100 and a smear was made. Slides were then incubated with FITC-PNA lectin (1:50, a gift from Dr. Peter Sutovsky), washed and mounted with VectorShield with DAPI (Vector Laboratories, Burlingame, CA).

Transmission electron microscopy (TEM)

Cauda epididymides were fixed in 4% PFA and 2.5% glutaraldehyde, contrasted with osmium tetroxide and embedded in resin. Ultrathin sections were cut and examined under a Hitachi H7600 TEM system.

Spermatocyte spread and immunolabeling

Spreading and immunolabeling protocols of testicular samples were performed as published elsewhere (Roig et al., 2010). Briefly, testes were dissected, rinsed in PBS and decapsulated. The remaining tissues were finely minced with a razor blade and transferred into 4 ml of separation medium (high glucose MEM with 1× proteinase inhibitor cocktail). Spermatocytes were released from the tubules by pipetting several times and debris allowed to settle for 5 min on ice. Spermatocyte suspension was then transferred to microcentrifuge tubes and spun down. Supernatants were removed and pellets were resuspended in 40 μl 0.1 M sucrose solution preheated to 37 °C. Twenty microliters of the mixture was added onto a glass slide preloaded with 65 μl 1% PFA (pH 9.2, also contains 0.1% triton X-100 and 1× proteinase inhibitor cocktail) and spread evenly across. Slides were incubated in a humidified chamber for two hours without disturbance, followed by rinsing in Photoflow solution (Kodak, 1:250). Air-dried slides were either stored at −80 °C or processed immediately. For immunostaining, slides were blocked in 0.2% BSA, 0.025% Tween-20 in 1× PBS for 10 min at room temperature, followed by incubation with primary antibodies overnight at 4 °C. On the following day, slides were washed and incubated with secondary antibodies for one hour, before being mounted with one drop of VectorShield with DAPI. Antibodies used are: SYCP1 (1: 200), SYCP3 (1:400) (both are kind gifts from C. Heyting, Wageningen University), γH2AX (1:800, Cell Signalling), RAD51 (1:100, Oncogene) and MLH1 (1:100, Pharmingen).

Testicular single-cell preparation for flow cytometry analysis and cell sorting

Isolation and staining of testicular cells were described previously (Getun et al., 2010; Lassalle et al., 2004; Vincent et al., 1998). Two to four million stained cells from one animal were diluted in 1 ml Gey's Balanced Salt Solution with Hoechst 33342 (Sigma-Aldrich, 5 μg/ml) before analysis. FACS analysis and cell sorting were performed on a DAKO MoFlo cell sorter described previously (Lassalle et al., 2004). Testes from three males of each genotype were analyzed individually and Student's t-tests were performed for each sub-population. Two-tailed p-value less than 0.05 is considered statistically significant.

Laser capture microdissection (LCM)

Epididymal tissues from *Prm*-Cre;*Cul4a*$^{c/c}$ male were fixed in 4% PFA, embedded in paraffin and sectioned at 6 μm. Slides were deparaffinized in three changes of xylenes, rehydrated in ethanol series and counter-stained with Mayer's Hematoxylin. Slides were then dehydrated in ethanol series, followed by three washes in xylenes and air dried briefly. The PixCell II LCM apparatus was used to microdissect spermatozoa from 8 to 10 sections (7.5 μm spot diameter) onto CapSure HS LCM caps (Arcturus, Mountain View, CA). Membranes with captured tissue were removed from LCM caps and digested in PBND buffer (50 mM KCl, 10 mM Tris–HCl pH 8.3, 2.5 mM $MgCl_2$, 0.1 mg/ml gelatin, 0.45% NP40, 0.45% Tween20) in the presence of 0.1 mg/ml Proteinase K overnight at 55 °C. The remaining tissues on the slide were scraped, digested and used as positive controls for PCR. Routine PCR was performed using primers oz618 (5′ATCGCCTTCCTACCCTTCTC3′) and oz628 (5′ATCCTTCTGCCTGTCTG-GAGT3′) for the *Cul4a* wild-type and floxed alleles; or oz618 and oz681 (5′-GTGAATGCTGAATCTAGCACC-3′) for the deleted allele.

Statistical analysis

Statistical analyses were performed with Microsoft Excel applying the Student's two-tailed t-test. Results are presented as average ± standard deviation. Differences in average values were considered significant with P-values less than 0.05.

Results

Dynamic CUL4A and CUL4B expression in developing and adult mouse testis

The CRL4 ubiquitin ligase activity is essential for cell viability, as deletion of the DDB1 adaptor of CRL4 in mice resulted in embryonic lethality (Cang et al., 2006), and simultaneous inactivation of both CUL4A and CUL4B is detrimental to cell growth and survival (Liu et al., 2009). Strikingly, *Cul4a*−/− mice displayed no overt developmental and growth defects, and had a normal life span, suggesting functional compensation from *Cul4b*. Because previous studies showed that knocking down the only *Cul4* in *C. elegans* led to premature entry into spermatogenesis (Zhong et al., 2003), we set out to test whether CUL4 proteins are also involved in mammalian spermatogenesis. First, we examined the expression of CUL4A and CUL4B at multiple time-points during the first round of spermatogenesis by double IF with antibodies against either CUL4 protein and PLZF, a marker for spermatogonial stem cells (Costoya et al., 2004). At P0, both CUL4 proteins are expressed in gonocytes, the primitive germ cells marked by nuclear PLZF staining (Fig. 1A and F, arrowheads). As gonocytes underwent proliferation and differentiation, CUL4A and CUL4B started to exhibit distinct expression patterns. CUL4A expression was detected in primitive A spermatogonia on P6 (Fig. 1B). By P12, CUL4A was detected in the newly emerged primary spermatocytes (Fig. 1C, asterisks), and its expression weakened in spermatogonia, especially in type A spermatogonia (Fig. 1C, arrowhead). By P14, CUL4A expression was confined to primary spermatocytes and was no longer detected in PLZF-expressing type A spermatogonia (Fig. 1D, asterisks and arrowheads, respectively). By P24, when the first round of spermatogenesis is almost complete, CUL4A was predominantly detected in primary spermatocytes in the pachytene/diplotene stage (Fig. 1E, asterisks), with residual CUL4A protein, if any, detected at earlier or later stages (Supplemental Fig. S1A and B). Note that CUL4A expression was low in tubules containing mostly spermatids (Fig. 1E, arrow), but high in tubules containing primary spermatocytes (Fig. 1E, asterisks). CUL4B expression, on the other hand, persisted in primitive A spermatogonia (Fig. 1G, arrowhead) and more differentiated spermatogonia (Fig. 1H, arrowheads). Its expression was gradually downregulated in emerging zygotene spermatocytes due to meiotic sex chromosome inactivation (MSCI) as *Cul4b* is on the X-chromosome (Fig. 1H, open arrowhead, inside dashed line). Concordantly, CUL4B expression was absent in pachytene/diplotene spermatocytes (Fig. 1I) and reappeared in newly formed round spermatids at P24 (Fig. 1J, asterisks, Fig. S1C and D). In addition, CUL4B was also detected in Sertoli cells throughout postnatal development (arrows in Fig. 1G and I).

In adult testes, both CUL4 proteins and mRNAs continued to exhibit a phase-specific expression pattern as revealed by IF and in situ hybridization, respectively (Fig. 1K, P and data not shown). CUL4A expression started to elevate in primary spermatocytes after they entered mid-pachytene phase (Fig. 1L), peaked in late pachytene phase (stages VII–VIII), and gradually declined afterwards (Fig. 1K). The protein was not detected in spermatids beyond step 5 based on seminiferous tubule staging as described previously (Fig. 1M, arrows) (Russell, 1990), nor was it present in Sertoli cells or spermatogonia marked by GATA-1 and PLZF, respectively (Fig. 1N and O). In contrast, CUL4B expression was mainly detected in Sertoli cells (Fig. 1Q, arrows), spermatogonia and round spermatids (Fig. 1Q, R, arrowheads and asterisks, respectively), where CUL4A was either absent or low in abundance. Overall, CUL4A and CUL4B exhibited a mostly complementary expression pattern in adult testis (Fig. 1S). DDB1, the DNA damage binding protein which forms ubiquitin ligase complex with both CUL4 proteins, was detected in virtually all testicular cell types with peak expression detected in mid-pachytene spermatocytes (Fig. S1E).

Cul4a null males are infertile

As *Cul4b*-null mouse has yet to be generated, we focused our study on *Cul4a* null animals to further explore its role during spermatogenesis. Absence of full-length CUL4A protein in the null testes was confirmed by Western blotting (Fig. S2A). In addition, PCR-genotyping further confirmed complete removal of the targeted exons (Fig. S2D). To assess *Cul4a* mutant fertility, six *Cul4a*+/− and nine *Cul4a*−/− adult males (10 weeks or older) were individually bred to wild type adult females. Vaginal plugs were recorded and the number of pups born was scored. The number of vaginal plugs detected in females was comparable between the two male genotypes. However, none of the females (36 total) mated with *Cul4a*−/− males were impregnated and produced any pups (Table 1). Female fertility was also tested and no difference was found between *Cul4a*−/− and their heterozygote littermates (Table 1). We did not detect any difference between *Cul4a*+/− and wild type mice in terms of fertility, testis morphology and sperm viability. Thus *Cul4a*+/− mice were used as controls in this study.

Morphological and histological analyses of Cul4a null testes

Anatomical examination revealed that the mutant testes, even though properly descended, were markedly reduced in size compared to those of the *Cul4a*+/− mice (Fig. S3A). Nevertheless, the rest of the internal male reproductive organs including the epididymides, vas deferens and seminal vesicles exhibited no gross difference between the two genotypes. H&E staining of mutant testis sections showed decreased diameters of seminiferous tubules, agenesis of germ cells, and increased interstitial tissues (Fig. 2B). Seminiferous tubules at various stages were evident in sections from control testes. On the other hand, *Cul4a*−/− tubules contained much fewer spermatids. Some tubules were degenerating while others showed accumulation of primary spermatocytes (Fig. S3D–E). The identity of primary spermatocytes was further confirmed by IF staining against CUL4A and PCNA, both shown to be specifically expressed in these cells (Kang et al., 1997). Since the CUL4A antibody we used for immunostaining recognizes the N-terminus of CUL4A, it would also label the mutant C-terminal truncated protein (CUL4AΔ), which was

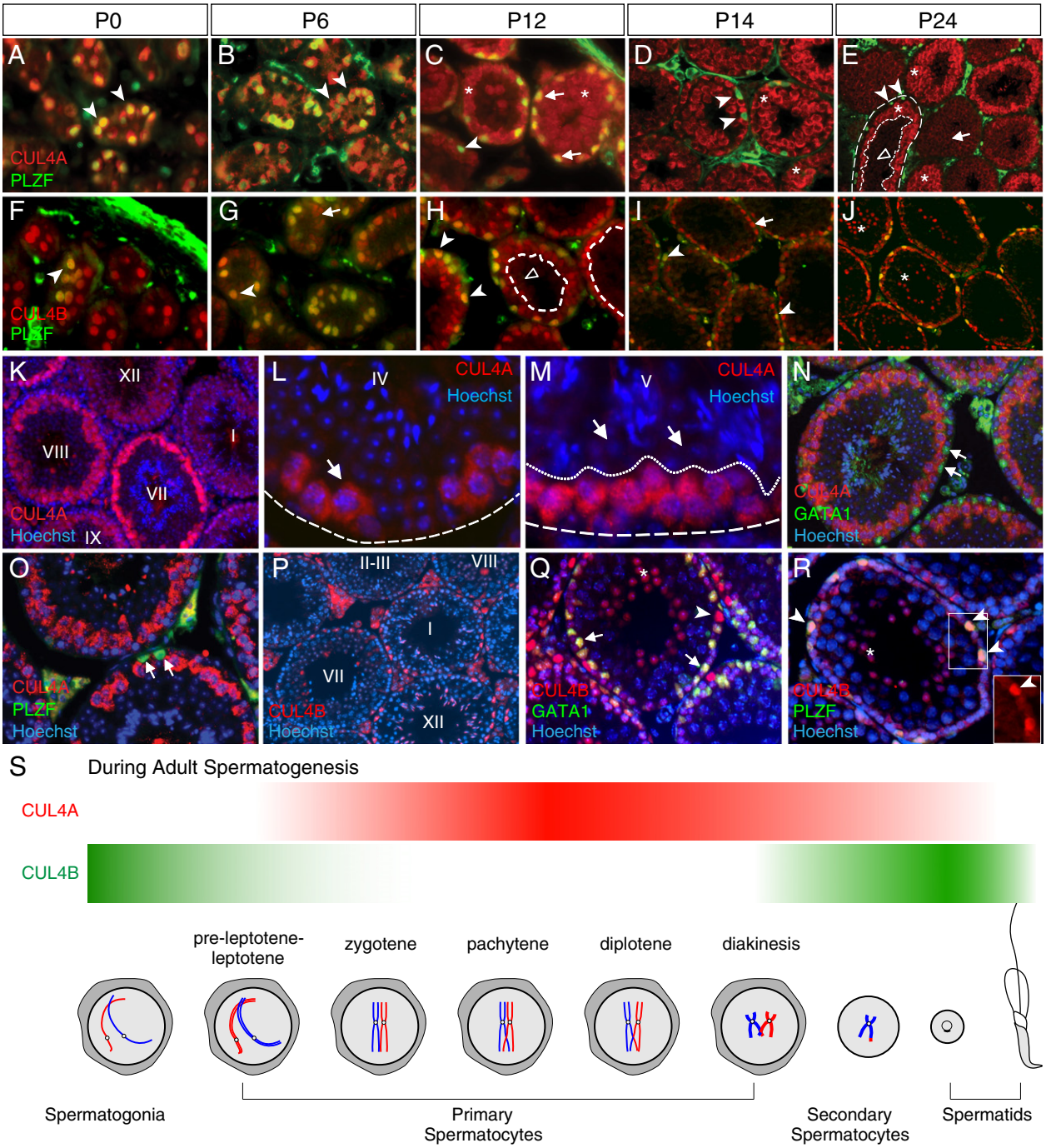

Fig. 1. Expression of CUL4A and CUL4B in developing and adult testes. (A–E) IF of CUL4A (red) and PLZF (green) on postnatal and peri-pubertal testes. CUL4A was present in gonocytes at P0 (A, arrowheads) and in primitive A spermatogonia at P6 (B, arrowheads). Its expression weakened in some A spermatogonia at P12 (arrowhead), and elevated in most B spermatogonia (arrows) and primary spermatocytes (asterisks) (C). At P14 and P24, CUL4A expression was only detected in primary spermatocytes (asterisks), but not in spermatogonia (arrowheads) (D and E). Note that dashed lines outline a seminiferous tubule in E; round spermatids inside the dotted lines do not express CUL4A; arrowheads point to quiescent A spermatogonia; arrow points to a tubule containing mostly spermatids with overall low CUL4A staining (E). See Fig. S1 for magnified images with nuclear staining. (F–J) CUL4B (red) and PLZF (green) expression during the first round of spermatogenesis. CUL4B was detected in gonocytes at P0 (F, arrowhead), in primitive A spermatogonia and more differentiated spermatogia (G, H, arrowheads). Expression gradually disappeared in primary spermatocytes (H, cells enclosed in dashed lines, open arrowhead). Its expression was restricted mainly to the spermatogonia and Sertoli cells at P14 (I, arrowheads and arrow, respectively), but was reactivated in round spermatids at P24 (J, asterisks). Arrows in panels G and I point to Sertoli cells. (K) IF of CUL4A (red) in adult testis (stages indicated as Roman numerals). CUL4A was present prominently in late-pachytene to diplotene spermatocytes of stage VII–IX tubules. (L) Pachytene spermatocytes (arrow) began to elevate CUL4A expression at stage IV (dashed line outlines the seminiferous tubule). (M) CUL4A was no longer detected in step 5 spermatids (arrows, dotted line outlines the boundary between spermatocytes and spermatids). (N) Double IF of CUL4A (red) and GATA1 (green) showed no CUL4A in Sertoli cells (arrows). (O) Double IF of CUL4A (red) and PLZF (green) showed no CUL4A expression in quiescent spermatogonia (arrows). (P) IF of CUL4B in adult testis detected the protein mainly in Sertoli cells, spermatogonia and spermatids. (Q, R) Double IF of CUL4B with GATA1 or PLZF showed its expression in Sertoli cells (Q, arrows) and in undifferentiated spermatogonia (R, arrowheads, inset), respectively and spermatids are marked by asterisks. (S) Diagram of the complimentary expression pattern of CUL4A and CUL4B during spermatogenesis in adult mice. The stages of each seminiferous tubule were determined according to Russell(1990).

Table 1
Fertility test of Cul4a−/− males and females. Adult males of Cul4a+/− or Cul4a−/− genetic background were mated to wild type female 2 months of age or older. Copulation was evidenced by presence of vaginal plug, and the date recorded. Of the 6 heterozygous males, over a time span of two months, all had copulated with 2–3 females, altogether giving rise to 15 litters with an average size of 10.5 pups. Even though vaginal plugs were observed in all 36 females bred to Cul4a−/− males, none of them were impregnated. Cul4a−/− females exhibited no signs of infertility, producing similar sized litters as their heterozygous littermates.

Males (n)	Females (n)	No. of vaginal plug observed in two months	No. of litters	No. of pups	Average litter size
Cul4a+/− (6)	*Cul4a*+/+ (17)	17	15	157	10.5
Cul4a−/− (9)	*Cul4a*+/+ (36)	65	0	0	0
Cul4a+/− (2)	*Cul4a*+/− (6)	9	8	73	9.1
Cul4a+/− (3)	*Cul4a*−/− (8)	13	10	87	8.7

previously proven to be non-functional (Liu et al., 2009). We thus used it as a marker for primary spermatocytes past the mid-pachytene phase in the mutant testis. The results clearly showed accumulation of CUL4AΔ-positive as well as PCNA-positive cells in mutant seminiferous tubules, demonstrating accumulation of mutant germ cells at the primary spermatocyte stage (Fig. S4). In addition, based on a previously established side-population detection method (Lassalle et al., 2004), we performed FACS analyses on 2–6 month old mutant and control testes and showed an increase in pachytene/diplotene cell population in mutant testis (19.1 ± 4.6% vs. 8.0 ± 1.7% in heterozygote controls, n = 3, p = 0.011), but not in cells at earlier stages (Fig. 2C, D, numbers represent average percentile ± standard deviation at each stage). These results demonstrated accumulation of primary spermatocytes at pachytene/diplotene stages in *Cul4a* mutants.

To assess spermatid development, we performed periodic acid-Schiff (PAS) staining to highlight acrosome granules. As shown in Fig. 2E and G, spermatids at all stages were present in *Cul4a*+/− testes, which were identifiable by their characteristic PAS staining pattern (Fig. 2G, arrows) (Russell, 1990). In contrast, much fewer PAS-positive spermatids were detected in *Cul4a*−/− seminiferous tubules (Fig. 2F) and it was impossible to stage the mutant spermatids due to their deranged PAS staining patterns indicative of abnormal acrosomes (Fig. 2H, arrows). It is noteworthy that the testis phenotype was observed as early as postnatal day 27, toward the end of the first round spermatogenesis, where round spermatids were evident in control animals but lack in number in the mutant. These results demonstrated that loss of CUL4A leads to defects in primary spermatocyte development and perturbed spermiogenesis, and suggest that CUL4A is required for meiotic progression of male germ cells.

Prolonged association of MLH1 with synaptonemal complexes in Cul4a−/− spermatocytes

The accumulation of pachytene/diplotene cells observed in *Cul4a*−/− prompted us to look into one of the key events in meiotic prophase I, the synaptonemal complex (SC) assembly. We examined SYCP1 and SYCP3 expression by immunostaining. SYCP1 is a member of the central element of the SC, whereas SYCP3 is a member of the lateral element. In normal pachytene spermatocytes, 19 autosomal SCs double-labeled with both SYCP1 and SYCP3 antibodies were detected whereas the sex body was mainly stained by SYCP3 only (Fig. 3A). As meiosis proceeded and cells entered diplonema, SYCP1 expression diminished and SCs were mostly dissociated (Fig. 3B). Even though normal SC assembly and disassembly were observed in many *Cul4a*-null primary spermatocytes (Fig. 3C, D), a fraction (~10–20%) of mutant cells exhibited abnormal SC structures at pachytene (Fig. 3G) and diplotene stages (Fig. 3H,I). In these cells, overall SYCP3 staining was stronger and we observed spotted SYCP3 staining which was not observed in controls. To assess homologous recombination events in primary spermatocytes, spreads were stained with RAD51 and γH2AX, together with SYCP3. RAD51 is a component of the early recombination nodule and many discrete RAD51 foci were detected along the SCs in leptotene and zygotene nuclei (Ashley et al., 1995), which declined in pachytene and diplotene cells (Fig. S5A–E). γH2AX, a histone modification that rapidly occurs in the vicinity of DNA double-strand breaks (DSBs), was present homogeneously in leptotene to zygotene nuclei, but was only detected in the sex body in late pachytene and diplotene cells (Fig. S5F–J) (Mahadevaiah et al., 2001). Neither RAD51 nor γH2AX showed any change in distribution in *Cul4a*−/− spermatocytes (Fig. S5A′–E′, F′–J′), indicating normal initiation and progression of early recombination events in the mutant.

Foci of the DNA repair protein MLH1 form along the SCs in pachytene cells, with at least one focus per SC. These foci mark recombination events (Baker et al., 1996; Moens et al., 2002), and are present in pachytene but not in diplotene cells (Fig. 3J, K). Examination of *Cul4a*−/− spermatocytes revealed no apparent difference in MLH1 foci number compared to controls, however, 24.2% (N = 82) of mutant pachytene cells contained at least one SC that did not have any MLH1 foci, which was not common in controls (3.4%, N = 78, Fig. 3L, arrowheads). Moreover, most MLH1 foci were still present in mutant diplotene cells. Immunostaining clearly showed a prolonged MLH1 association with the SCs in *Cul4a* mutant diplotene cells, presumably at the chiasmata, which are the cytological manifestation of crossovers (COs) (Fig. 3M, arrowheads). On average, mutant diplotene cells still had 18.7 ± 4.7 (N = 65) MLH1 foci associated with the SCs, whereas nearly all MLH1 foci had disappeared in diplonema in controls (0.3 ± 0.6, N = 79). These results suggest that even though *Cul4a*−/− spermatocytes can successfully initiate homologous recombination, they have defects in CO formation and resolution of the late recombination nodule.

To evaluate diakinesis in mutant spermatocytes, metaphase spreads were prepared from cells isolated from *Cul4a*+/− and −/− testes followed by DAPI staining to visualize DNA. Most control spermatocytes at metaphase I had 20 pairs of homologous chromosomes (Fig. 3N). In contrast, *Cul4a*−/− cells frequently contained univalents (27.3 ± 5.3%, N = 54 from three animals) which were not sex chromosome-specific compared to heterozygote controls (9.2 ± 0.7%, N = 56 from three animals) (Fig. 3O). Mutant secondary spermatocytes at metaphase II were mostly abnormal, many of which contained heterochromatin structures densely stained by DAPI (Fig. 3Q, arrows). This phenotype, however, could be secondary to the prolonged prophase I in the mutant rather than a direct effect of CUL4A on metaphase II.

Excessive apoptosis in Cul4a-deficient primary spermatocytes

To uncover mechanism of germ cell agenesis in *Cul4a*−/− mice, we evaluated germ cell proliferation and apoptosis in these mutants. Proliferating cells were pulse-labeled by BrdU and visualized by immunohistochemistry. Compared to heterozygous controls, *Cul4a*−/− testis showed normal DNA incorporation in various cell types, including pre-leptotene primary spermatocytes and spermatogonia at S-phase (Fig. 4A, B). TUNEL assay, on the other hand, showed massive apoptotic cells in many mutant tubules, but not in *Cul4a*+/− controls (Fig. 4C, D, arrows). To reveal the identity of apoptotic cells, Bouin-fixed H&E-stained mutant testis sections were examined carefully and the stage of seminiferous tubules was determined by spermatogonial morphology according to Ahmed and de Rooij(2009). Tubules at earlier stages contained morphologically normal pachytene cells, characterized by chromatin patches in the nucleus and their larger size (Fig. 4E, arrows). Apoptotic pachytene cells (aP) were more eosinophilic and their nuclei tend to be more compacted (Fig. 4F, arrows). We detected most apoptotic cells in tubules at later stages (VIII–XI), among mid-pachytene to diplotene spermatocytes. Double IF of SYCP3 and TUNEL also revealed

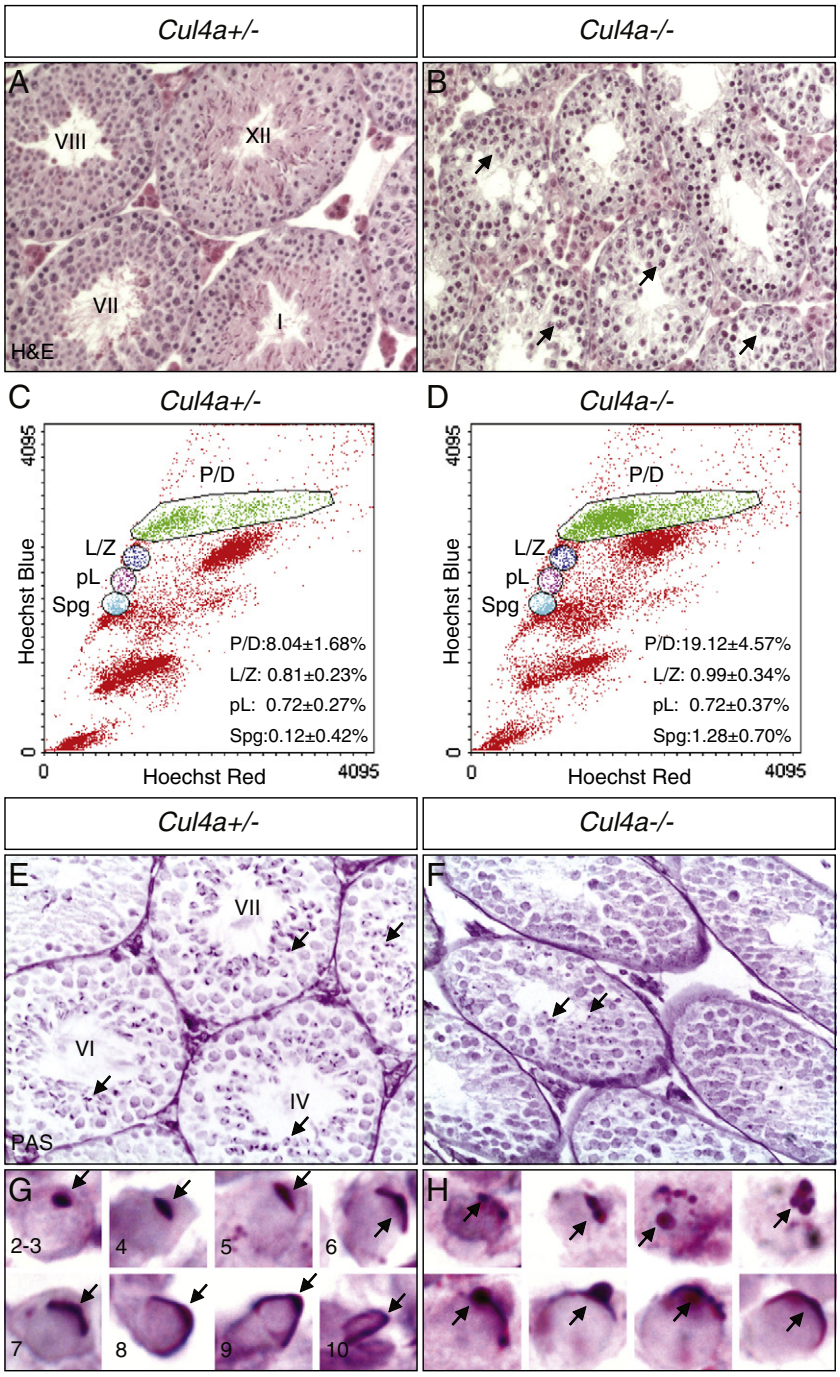

Fig. 2. Histology and morphology of *Cul4a*−/− testes. (A, B) H&E staining of testicular sections from *Cul4a*+/− and −/− mice revealed degeneration of seminiferous tubules in the mutant. Unlike the *Cul4a*+/− testis, where tubules at various stages were evident, *Cul4a*−/− tubules lacked stage-specific compositions of germ cells and contained accumulated pachytene/diplotene cells (arrows). (C, D) Representative images of FACS analysis of the Hoechst 33342-stained testicular cells revealed an increase in pachytene/diplotene cell population (green). P/D, pachytene/diplotene spermatocytes (19.12 ± 4.57% in mutants vs. 8.04 ± 1.68% in controls, $p = 0.011$, $n = 3$); L/Z, leptotene/zygotene spermatocytes (0.99 ± 0.34% in mutants vs. 0.81 ± 0.23% in controls, $p = 0.22$); pL, preleptotene spermatocytes (0.72 ± 0.37% in mutants vs. 0.72 ± 0.27% in controls, $p = 0.37$); Spg, spermatogonia (1.28 ± 0.70% in mutants vs. 1.12 ± 0.42% in controls, $p = 0.70$). Mutant mice 2–6 months of age and their heterozygous littermates were used for this analysis. (E) PAS assay identified round or elongated spermatids in every seminiferous tubule of the *Cul4a*+/− testis (arrows), and higher-magnification images of spermatids from steps 2–3 through step 10 were shown in G. Note that PAS-positive acrosomal structure gradually changed as spermatids matured (G, arrows). The mutant tubules contained only a limited number of PAS-positive cells (F) and exhibited abnormal acrosomal structures (H, arrows).

that these apoptotic cells had thread-like nuclear SYCP3 staining, confirming their pachytene/diplotene cell identity (Fig. 4F, inset).

Previous studies reported that the tumor suppressor p53 can stimulate a variety of signals which in turn act upon both the intrinsic and extrinsic apoptotic pathways to facilitate cell death (Vousden and Lane, 2007). Since extensive apoptosis was observed in *Cul4a*−/− spermatocytes, we speculated that p53 expression might be altered in these cells. Western blotting with whole testis lysates from control and mutant males revealed that although the total p53 level remained unchanged, phospho-p53 at Serine 15 was increased in the mutant (Fig. 4G). Elevation of phospho-p53 at Ser15 could reflect activation of upstream ATM/ATR pathway. However, no apparent changes were detected in phospho-CHK1 or CHK2 levels, known targets for ATM/ATR (Fig. S6). In addition, Western blotting and IF of γH2AX also confirmed

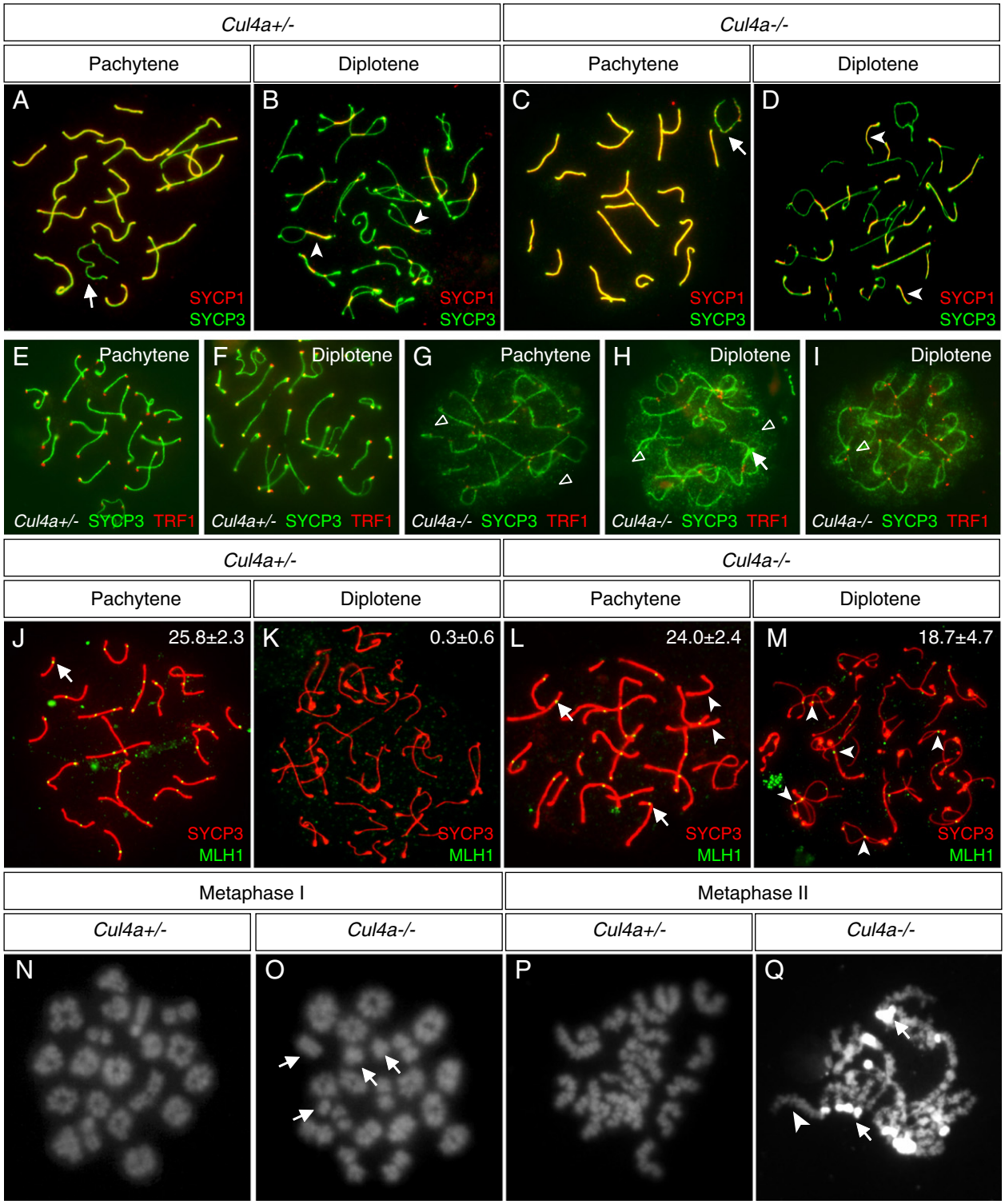

Fig. 3. Characterization of prophase progression in *Cul4a*−/− spermatocyte spread. (A–D) Double IF of SYCP1 and SYCP3. (A) In pachynema, autosomal SCs appeared as univalent structure stained by both SYCP1 (red) and SYCP3 (green), which labeled the central and axial elements of the SC, respectively. The sex body had minimal double-labeled region, due to large non-homologous regions on the X and Y chromosomes (arrow). As prophase proceeded to the diplotene stage, SCs started to disassemble whereby bivalent structures highlighted by SYCP3 staining were only connected at the "crossing overs", which retained SYCP1 staining (B, arrowheads). Even though a similar SYCP1/3 staining pattern was observed in many *Cul4a*−/− primary spermatocytes (C, D), about 10–20% of mutant cells exhibited abnormal SC structures (G–I). Double IF of SYCP3 (green) and TRF1 (red) stained control pachytene (E) and diplotene (F) spermatocytes. (G–I) Mutant primary spermatocytes often exhibited strong spotty nuclear SYCP3 staining (open arrowheads) and regions with stronger SYCP3 staining (arrows). (J) DNA repair protein, MLH1 (green), formed discrete foci along the SCs stained by SYCP3 antibody (red) in pachytene spermatocytes (arrows). The foci were no longer detectable in diplotene spermatocytes of the *Cul4a*+/− testis (K). The number of MLH1 foci appeared normal in *Cul4a*−/− pachytene cells (L, arrow), however, 24.2% of mutant spermatocytes contained SCs that did not have any MLH1 focus (arrowheads point to SCs without MLH1 foci). Moreover, MLH1 foci remained on the SCs of the mutant diplotene spermatocytes, especially at the crossover sites where homologous chromosomes were still connected (M, arrowheads). Numbers in panels J–M represent the number of MLH1 foci at corresponding stages (average ± standard deviation). Representative pictures of M-phase spread from *Cul4a*+/− testes stained with DAPI showed normal number and shape of chromosomes at metaphase I (N) and metaphase II (P). The mutant, on the other hand, showed many cell spreads with univalent chromosomes at metaphase I (O, arrows), and atypical DNA staining of haploid metaphase II cells (Q). Note that mutant chromosomes were generally longer than controls and there were regions with highly-condensed DNA with strong DAPI staining (arrows). Arrowheads point to regions with relatively normal DNA staining.

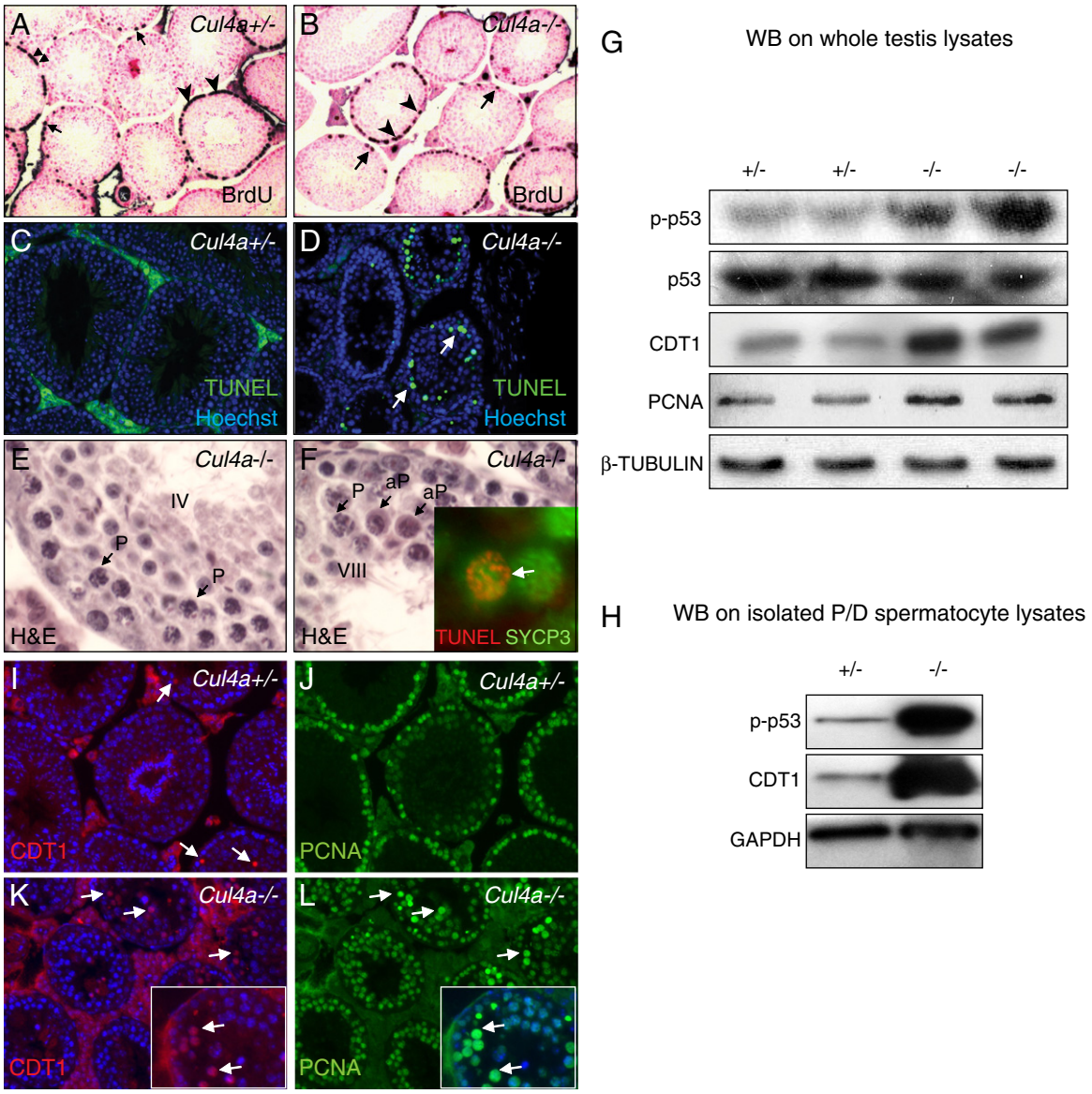

Fig. 4. Excessive apoptosis and accumulation of CDT1 in *Cul4a*−/− primary spermatocytes. (A, B) BrdU immunohistochemistry (black) showed no obvious difference in cell proliferation in either mitotic spermatogonia (arrows) or meiotic pre-leptotene primary spermatocytes (arrowheads) in *Cul4a*−/− testis. Cell nuclei were counter-stained with Nuclear Fast Red and appeared pink. (C, D) TUNEL assay showed a dramatic increase in the number of apoptotic cells inside *Cul4a*−/− seminiferous tubules (arrows). (E, F) H&E staining of mutant testis sections showed that pachytene cells in tubules at early stages were morphologically normal (E, arrows. P, pachytene spermatocytes), but many of those at later stages showed signs of apoptosis (F, arrows. aP, apoptotic pachytene spermatocytes). Double labeling showed that TUNEL-positive cells (red) also exhibited thread-like SYCP3 staining in the nucleus (green), characteristic of primary spermatocytes (F, inset, arrow). (G) Western blotting on whole testis lysates revealed accumulation of phospho-p53 (Ser15), CDT1 and PCNA protein in the mutant testes. No obvious changes were observed for total p53. (H) Western blotting on sorted pachytene/diplotene cells showed that p-p53 and CDT1 are enriched in these cells. β-tubulin and GAPDH served as loading controls for Western blots. Double IF of CDT1 and PCNA revealed sporadic CDT1 staining in a few primary spermatocytes in *Cul4a*+/− (I, arrows), however, an increased number of CDT1-positive cells were present in mutant tubules which also expressed elevated level of PCNA (K and L, arrows). Images at higher-magnification were shown in K and L insets.

no change in its expression level and distribution, indicating no gross alteration in the number of DSBs (Fig. S6). Western blotting of phospho-p53 on isolated pachytene/diplotene spermatocytes further demonstrated that its accumulation was contributed mainly by this cell population (Fig. 4H). This elevated p53 activity is likely the underlying cause for the increased apoptosis in mutant spermatocytes.

In *C. elegans*, absence of *Cul4* resulted in perturbed spermatogenesis which is associated with accumulation of the DNA-replication licensing protein, CDT1 (Zhong et al., 2003), a direct target of DDB/Cul4-mediated ubiquitination. In mammals, CDT1 has been reported to be highly expressed in a subset of primary spermatocytes, even though DNA synthesis at this stage has long ceased. This raised the possibility that besides DNA replication licensing, CDT1 may be involved in other processes such as homologous recombination, DNA repair or meiotic progression. To determine whether CDT1 is affected in *Cul4a*−/− testis, we examined its expression, as well as that of PCNA, the cofactor for CDT1 degradation by the DDB/CUL4 complex (Arias and Walter, 2006). In control testis, PCNA was mostly confined to primary spermatocytes (Fig. 4J), and sporadic CDT1 staining was detected (Fig. 4I, arrows). In mutant testis, however, an increased number of CDT1-expressing cells were evident in many seminiferous tubules, most of which also showed markedly elevated level of PCNA (Fig. 4K, L, arrows). Western blotting against CDT1 also confirmed its accumulation in the mutant, particularly in pachytene/diplotene cells (Fig. 4G, H). These data indicate that CDT1 is also a target of CUL4A in mammalian spermatocytes and accumulation of CDT1 could contribute to the mutant meiotic defects.

To address whether CUL4B is ectopically induced to compensate for the loss of CUL4A, we examined CUL4B expression in *Cul4a*−/− testis. Western blotting of CUL4B on testis lysates revealed no significant difference in protein levels between *Cul4a*+/− and *Cul4a*−/− mice (Fig. S2B). IF showed that *Cul4a*−/− testis contained much fewer CUL4B-expressing spermatids, but more importantly, CUL4B was not ectopically induced in primary spermatocytes, indicating normal MSCI in *Cul4a* mutants (Fig. S6E, F). These results indicate that loss of CUL4A is not compensated by CUL4B in *Cul4a*−/− primary spermatocytes, and that lack of any CUL4 protein in these cells ultimately leads to defects in meiotic progression.

Cul4a−/− male mice exhibited oligoasthenospermia and spermatozoa malformation

While many *Cul4a*−/− germ cells accumulated at pachynema/diplonema and subsequently underwent apoptosis, some did proceed to later stages. To evaluate the number and motility of mature mutant sperms, we first performed Computer-Assisted Sperm Analysis (CASA) on sperm samples harvested from the caudal epididymis of *Cul4a*−/− and control males. As expected, a prominent decrease in sperm count was found in the mutant (12.9 million/ml), compared to those in wild-type and *Cul4a*+/− (51.0 and 53.8 M/ml, respectively, Fig. 5A, $n=3$, $P=0.004$). The majority of sperms from both wild-type and *Cul4a*+/− mice were rapid-moving (88.6% and 82.0%). In contrast, more than half of the mutant sperms were static (Fig. 5B). To examine mutant sperm morphology, sperm smears were prepared and stained with H&E. Sperms from heterozygous males showed normal morphology, with distinct head (acrosome and nucleus) and tail (mid-, principle- and end-pieces) structures (Fig. 5C). On the other hand, most *Cul4a*−/− sperm heads contain a condensed nucleus but lacked a defined acrosome. Their tails were usually composed of a thin or fragmented mid-piece, an occasionally kinked principle piece and a less affected end piece. To further characterize the structure of the head and mid-piece, live sperms were incubated with MitoTracker, an orange fluorescent dye that stains active and functional mitochondria, followed by staining with FITC-labeled lectin PNA, which selectively binds to acrosomes. As shown in Fig. 5D, normal sperms contained a sickle-shaped head (magenta), an acrosomal cap overlying the anterior contour of the head (green), and a mid-piece that was covered by a mitochondrial sheath (red). The mutant sperms, however, exhibited a wide spectrum of abnormalities including disorganized or completely absent acrosomal structure, disintegrated or lack of mitochondrial sheath, and aberrant head shape (Fig. 5D, b–d′). Ultrastructural study by transmission electron microscopy (TEM) revealed that in addition to the lack of an acrosomal structure, mutant sperms often displayed characteristics of Dysplasia of the Fibrous Sheath (DFS), including absence of axonemes and/or outer dense fibers as well as distorted longitudinal columns (Fig. 5E). These results demonstrated that *Cul4a*−/− sperms lacked active mitochondrial sheaths and normal acrosomes, which should severely compromise their motility and their ability to penetrate the zona pellucida of the egg, rendering the mutant males infertile.

We next asked whether mutant sperms can fertilize oocytes in close proximity by performing in vitro fertilization (IVF) as described previously (Kim and Moley, 2008), thereby bypassing the quantity and mobility issues. Greater than 80% of oocytes were fertilized and developed to 2-cell stage by either wild-type or *Cul4a*+/− sperms, whereas only 10.4% of eggs (24 out of 231) did so after incubation with mutant sperms (Fig. 5F, H). Moreover, only two eggs fertilized by mutant sperms progressed to blastocysts compared to more than 60% in controls (Fig. 5G, H). Taken together, these results indicated that the infertility phenotype in *Cul4a*−/− males reflected a series of defects in spermatozoa including reduced number and motility, and compromised acrosome reaction. Furthermore, the fact that the few oocytes fertilized by *Cul4a*−/− sperms could not thrive indicated potential chromosomal deficiencies carried by most mutant sperms in addition to their morphological defects.

Even though the spermatogenesis defects observed in *Cul4a*−/− mice may largely be due to meiotic prophase progression failure, it is possible that CUL4A also plays a role during spermiogenesis. Although CUL4A expression was markedly reduced after the diplotene stage (Fig. 1K), residual CUL4A protein may be required during later stages of spermatogenesis. To begin addressing this, *Cul4a* conditional knockouts were generated using the *Prm*-Cre which presumably drives Cre expression in round spermatids. *Prm*-Cre; *Cul4a*$^{c/c}$ males did not exhibit any fertility defects. Histological analysis of the mutant testis revealed normal progression of spermatogenesis (Fig. S7). Although complete deletion of the *Cul4a* gene was confirmed by PCR of genomic DNA extracted from LCM-captured spermatozoa, we were unable to confirm loss of wild type CUL4A protein during spermiogenesis due to technical difficulty. Hence the role of CUL4A in mouse spermiogenesis requires further investigation.

Discussion

Spermatogenesis is a complicated process involving mitotic cell division, meiosis and spermiogenesis. In order for germ cells to progress through these steps, protein degradation has to be tightly regulated. In this paper, we systematically studied the function of the *Cul4a* gene, which encodes a Cullin-RING ubiquitin ligase, in spermatogenesis and demonstrated that *Cul4a*-mediated protein degradation is essential for the maturation of primary spermatocytes.

Germ-line deletion of *Cul4a* in the mouse affects neither embryonic development nor growth and life span of the animal, likely due to redundant *Cul4b* expression in most tissues (Liu et al., 2009). Here we demonstrate that *Cul4a*-deficient males are infertile. The testes of adult mutants are smaller, and contain more pachytene primary spermatocytes but much fewer germ cells beyond the diplotene stage in the seminiferous tubules. As a result, the mutants produce much less mature spermatozoa, most of which exhibit morphological defects mainly in the head and mid-piece regions, rendering them immotile and unable to fertilize eggs even in vitro. This stage-specific accumulation is consistent with high CUL4A expression in pachytene cells, suggesting a cell autonomous requirement for CUL4A in prophase I.

Our molecular analysis using a panel of markers labeling synaptonemal complexes (SYCP1/SYCP3) and early homologous recombination events (RAD51/γH2AX) show largely normal SC assembly, initiation and repair of DSBs in the mutants. Contrary to recent findings using a different *Cul4a* allele which showed persisted γH2AX foci in *Cul4a*−/− spermatocytes (Kopanja et al., 2011), no apparent defects in DNA double strand break repair were observed by either RAD51 or γH2AX staining (Fig. S5) in our system, indicating that early steps of homologous recombination are not affected by CUL4A deletion. Nevertheless, the mutant cells exhibit a prolonged MLH1 association with SCs, which strongly suggests a defect in CO resolution. *Mlh1* is the vertebrate homolog of the *Escherichia coli* DNA mismatch repair gene *mutL*, and was identified as frequently mutated in hereditary nonpolyposis colon cancer (Bronner et al., 1994). Mutation of *Mlh1* in the mouse causes both male and female sterility. Mutant male germ cells arrest at metaphase I and are mostly eliminated through apoptosis, indicating important roles for *Mlh1* in prophase progression (Baker et al., 1996). The fact that MLH1 foci are present in many late-pachytene and diplotene mutant cells, a novel phenotype that has not been previously observed in other meiosis animal models, indicates a failure of recombination nodule resolution. The mechanism responsible for degradation of MLH1 is currently unknown, but it is unlikely a direct DDB-CUL4A target because we did not observe MLH1 accumulation in *Cul4a*−/− pachytene/diplotene lysates (data not shown). Instead, MLH1 perdurance may reflect defect(s) in events prior to or during CO resolution. Examination of several proteins critical to this process, including BLM helicase and BTBD12/Slx4 endonuclease (Oh et al., 2007;

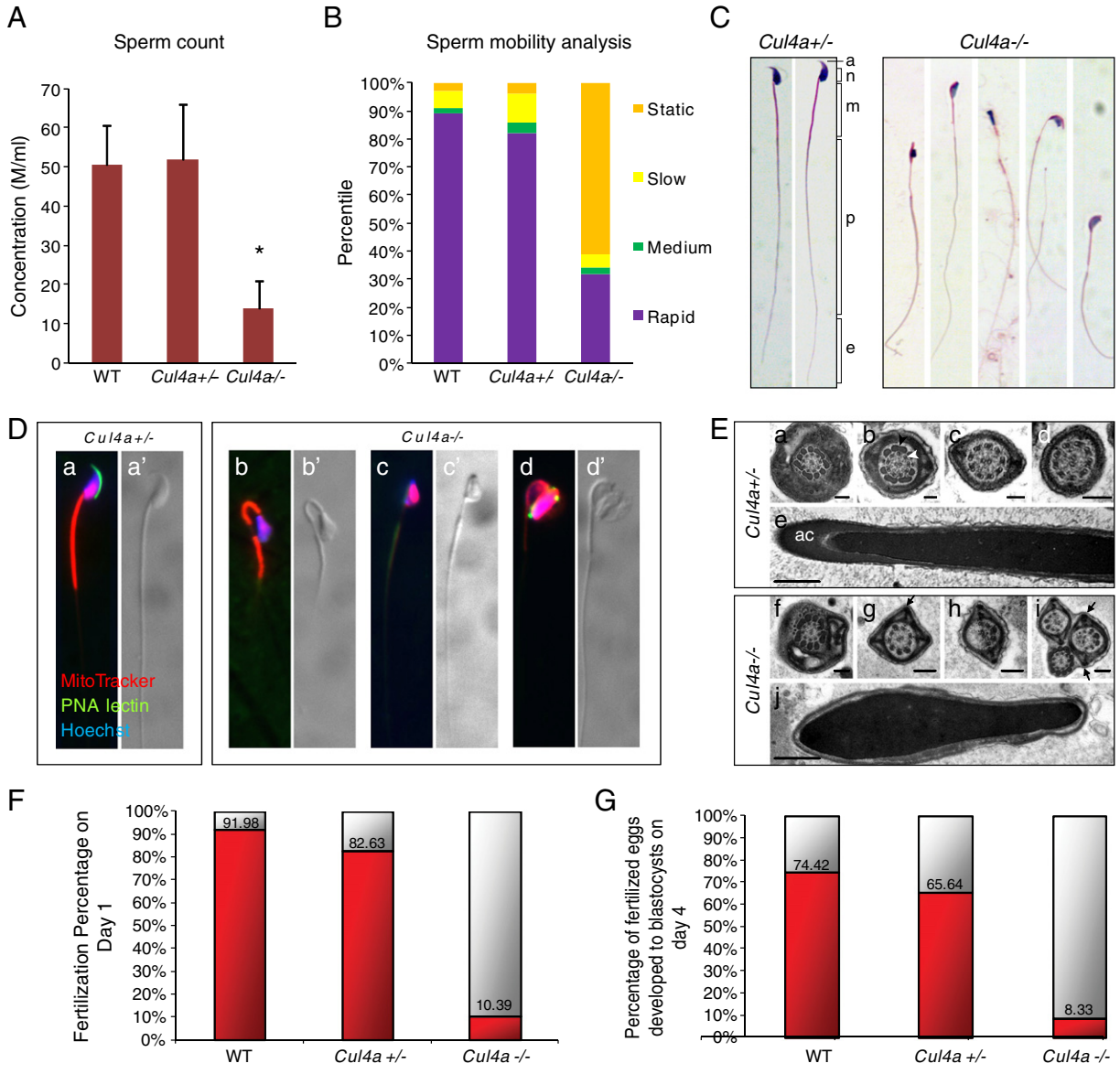

H

male genotype	total WT oocytes used	# of oocytes fertilized on day 1	% fertilization	# of oocytes developed to blastocysts on day 4	% of oocytes developed to blastocysts on day 4
WT	187	172	91.98	128	74.42
Cul4a +/-	236	195	82.63	128	65.64
Cul4a -/-	231	24	10.39	2	8.33

Fig. 5. Count, motility and morphology of *Cul4a*−/− sperms. (A) A dramatic reduction in epididymal sperm number in *Cul4a*−/− compared to either wild type or heterozygotes (n = 3 for each genotype). Asterisk: P value = 0.004 (controls vs. mutants). (B) CASA revealed that the majority of both wild type and *Cul4a*+/− sperms were rapidly moving, whereas 56.5% of mutant sperms were motionless. (C) H&E staining of the sperm spread showed a hematoxylin-positive head and an eosin-positive acrosome and tail in heterozygote sperms, whereas mutant sperms were phenotypically abnormal. a, acrosome; n, nucleus; m, mid-piece; p, principle piece; e, end piece. (D) Analysis of sperm sub-structures by staining with the MitoTracker (mid-piece and part of head, red), lectin PNA (acrosome, green) and DAPI (head, blue). A phase-contrast picture of the same sperm was displayed next to the fluorescent photo. Typical sperms have sickle-shaped head with strong MitoTracker staining in the mid-piece and well-defined lectin staining was evident in controls. The mutant sperms, however, generally lacked lectin staining and mitochondrial staining in the mid-piece, or had a fragmented mid-piece. (E) Transmission electron microscopy confirmed the lack of acrosomal (ac) structures in the mutant sperm heads (j). In addition, mutant sperms were often missing the axenemal microtubule doublets (white arrowheads, compare h and i to b–d) and corresponding outer dense fibers (black arrowheads, compare i to b–d). Additional or not properly opposed longitudinal columns were also observed in many mutant sperms (g, i, arrows). Scale bars in E: 100 nm. (F–H) IVF results using super-ovulated wild-type oocytes and sperms isolated from wild type, *Cul4a*+/− or *Cul4a*−/− caudal epididymal sperms. (F) On day 1 following IVF, 91.2% and 82.6% of oocytes were fertilized by wild type and *Cul4a*+/− sperms, respectively, as they progressed to 2-cell stage. Only 10.4% oocytes did so with *Cul4a*−/− sperms. (G) 74.4% (wild type) and 65.6% (*Cul4a*+/−) of the 2-cell stage embryos further developed to blastocysts in culture, whereas only 8.3% embryos resulted from mutant sperms did. (H) Summary of the number of oocytes/zygotes/embryos at different stages during IVF. Three males of each genotype were used in this experiment.

Svendsen et al., 2009) could help further clarify the role of CUL4A in this process. It is also possible that in *Cul4a*−/− spermatocytes there is uncoupling of CO formation/resolution and SC dissociation. In other words, SCs prematurely desynapse, making mutant pachytene spermatocytes look like diplotene cells. We rule out this possibility by immunostaining of phospho-histone H3 (Ser10), a modification starting in late diplonema (Cobb et al., 1999), together with SYCP3. The result shows normal progression of SC disassembly in mutant diplotene spermatocytes (Fig. S8).

It is noteworthy that even though *Cul4a*−/− spermatocytes show normal total number of MLH1 foci at pachynema, a fraction of these mutant cells do contain SCs that lack MLH1 focus/foci, which reflects an earlier defect in CO formation. Even though the cause of this defect and the potential involvement of CUL4A during CO formation are not known, this failure to establish COs on every SC may have caused the univalent chromosomes observed in mutant metaphase I spermatocytes (Fig. 3L). In addition to the morphological abnormalities seen in *Cul4a*−/− spermatozoa, these chromosomal defects may also contribute to infertility.

CDT1, a DNA replication licensing protein, is a known DDB1/CUL4 complex target. In mitotic cells, CDT1 level peaks in G1 phase and declines precipitously during S phase through timely degradation (Hofmann and Beach, 1994). Inactivation of *Cul4* as well as *Ddb1* in *C. elegans* leads to CDT1 accumulation in somatic cells and results in re-replication of the genome (Hu et al., 2004; Kim and Kipreos, 2007), and its accumulation may also be related to the premature spermatogenesis phenotype in *Cul4* knockdown *C. elegans* mutants (Kim and Kipreos, 2007). In the mouse, the expression and function of CDT1 in spermatogenesis has not been systematically investigated. We found that CDT1 protein is expressed in a small fraction of primary spermatocytes (Fig. 4I), and its expression is extremely low in CUL4A-expressing pachytene/diplotene spermatocytes. In *Cul4a* mutants, we observed ectopic CDT1 in pachytene/diplotene primary spermatocytes supporting that CDT1 is a direct target of CUL4A in mouse germ cells. Consistent with studies in *C. elegans* (Kim et al., 2007), our FACS analysis on the mutant testes show no evidence of DNA re-replication. In addition, MCM7, one of the key components that form the pre-replication complex with CDT1 to initiate DNA replication, was present in whole testis lysates (Fig. S6G) but absent in lysates from purified pachytene/diplotene cells of either control or mutant mice (data not shown). These findings suggest an unconventional role for CDT1 in mammalian spermatocytes other than regulating DNA replication.

The perdurance of MLH1 foci may reflect defects in meiotic cell cycle progression. The tumor suppressor gene *p53*, also known as the guardian of the cell cycle, was shown to be expressed in primary spermatocytes and associated with meiotic cell-cycle progression and recombination repair (Beumer et al., 1998). It was hypothesized that p53 may regulate apoptosis of germ cells in response to genotoxic stress, since elimination of p53 homolog, *Cep1*, in *C. elegans* renders germ cells resistant to radiation-induced apoptosis (Derry et al., 2001). Indeed, we observed a marked increase in activated p53 protein, in *Cul4a*−/− testis. However, we did not observe any changes in the upstream ATM/CHK2 pathway in the mutant suggesting either that another upstream signal triggers p53 phosphorylation or that p-p53 is stabilized in the absence of *Cul4a*. Activation of p53 likely leads to excessive apoptosis of the mutant spermatocytes. Similarly, accumulated p53 protein was observed in DDB1 mutant ventricular zone which is responsible for the apoptosis of proliferating neural progenitor cells (Cang et al., 2006). Furthermore, previous studies in cultured mitotic human cells have shown that inactivation of CUL4A stabilizes intracellular p53 and causes cell growth arrest (Banks et al., 2006). It is possible that DDB1/CUL4A complex maintains p53 homeostasis in primary spermatocytes, and loss of CUL4A in germ cells likely triggers a pachytene checkpoint which leads to spermatocyte apoptosis.

Even though a large portion of mutant spermatocytes exhibited defects in progression through pachynema and subsequently eliminated via apoptosis, a few of them do proceed through meiosis and further developed into mature sperms. However, these mutant sperms exhibit a range of defects in virtually all parts of the sperm. It is most likely that these defects are secondary to prophase I progression defects, but we could not rule out the possibility that CUL4A function is also required for spermiogenesis in the current study.

The severe infertility phenotype observed in *Cul4a*-null male mice implicates indispensible functions for CUL4 proteins in meiosis. So why are female mutants spared from the catastrophic consequences of losing CUL4A? We reasoned that CUL4B protein, which is turned off by MSCI in male but not in female germ cells, is sufficient to ensure proper degradation of CUL4 target proteins and maintain meiotic progression in *Cul4a*−/− oocytes. In support of this hypothesis, both CUL4A and CUL4B are present in SYCP3-positive pachytene oocytes as revealed by IF analyses on E18.0 mouse ovary (Fig. S9). Therefore our data demonstrate the importance of DDB1/CUL4 machinery during spermatogenesis, and suggest a possible role in female meiosis as well.

Acknowledgments

We would like to thank Dr. Patricia Hunt for help with metaphase analysis; Dr. Peter Sutovsky for MitoTracker and PNA stains as well as help with phenotypic analysis and helpful suggestions; and Jaclynn Lett and the Research Center for Auditory and Vestibular Studies, Department of Otolaryngology at Washington University for technical assistance with electron microscopy. We also thank the Alvin J. Siteman Cancer Center at Washington University School of Medicine and Barnes-Jewish Hospital in St. Louis, MO, for the use of the High Speed Cell Sorter Core, which provided cell sorting service. The Siteman Cancer Center is supported in part by an NCI Cancer Center Support Grant #P30 CA91842. This work was supported by National Institutes of Health Grants ES014482 and ES016597 to L.M., and CA098210 and CA118085 to P.Z.

Appendix A. Supplementary data

Supplementary data to this article can be found online at doi:10.1016/j.ydbio.2011.05.661.

References

Ahmed, E.A., de Rooij, D.G., 2009. Staging of mouse seminiferous tubule cross-sections. Methods Mol. Biol. 558, 263–277.
Arias, E.E., Walter, J.C., 2006. PCNA functions as a molecular platform to trigger Cdt1 destruction and prevent re-replication. Nat. Cell Biol. 8, 84–90.
Ashley, T., Plug, A.W., Xu, J., Solari, A.J., Reddy, G., Golub, E.I., Ward, D.C., 1995. Dynamic changes in Rad51 distribution on chromatin during meiosis in male and female vertebrates. Chromosoma 104, 19–28.
Baker, S.M., Plug, A.W., Prolla, T.A., Bronner, C.E., Harris, A.C., Yao, X., Christie, D.M., Monell, C., Arnheim, N., Bradley, A., Ashley, T., Liskay, R.M., 1996. Involvement of mouse Mlh1 in DNA mismatch repair and meiotic crossing over. Nat. Genet. 13, 336–342.
Banks, D., Wu, M., Higa, L.A., Gavrilova, N., Quan, J., Ye, T., Kobayashi, R., Sun, H., Zhang, H., 2006. L2DTL/CDT2 and PCNA interact with p53 and regulate p53 polyubiquitination and protein stability through MDM2 and CUL4A/DDB1 complexes. Cell Cycle 5, 1719–1729.
Baudat, F., Manova, K., Yuen, J.P., Jasin, M., Keeney, S., 2000. Chromosome synapsis defects and sexually dimorphic meiotic progression in mice lacking Spo11. Mol. Cell 6, 989–998.
Beumer, T.L., Roepers-Gajadien, H.L., Gademan, I.S., van Buul, P.P., Gil-Gomez, G., Rutgers, D.H., de Rooij, D.G., 1998. The role of the tumor suppressor p53 in spermatogenesis. Cell Death Differ. 5, 669–677.
Bronner, C.E., Baker, S.M., Morrison, P.T., Warren, G., Smith, L.G., Lescoe, M.K., Kane, M., Earabino, C., Lipford, J., Lindblom, A., et al., 1994. Mutation in the DNA mismatch repair gene homologue hMLH1 is associated with hereditary non-polyposis colon cancer. Nature 368, 258–261.
Cang, Y., Zhang, J., Nicholas, S.A., Bastien, J., Li, B., Zhou, P., Goff, S.P., 2006. Deletion of DDB1 in mouse brain and lens leads to p53-dependent elimination of proliferating cells. Cell 127, 929–940.
Cobb, J., Miyaike, M., Kikuchi, A., Handel, M.A., 1999. Meiotic events at the centromeric heterochromatin: histone H3 phosphorylation, topoisomerase II alpha localization and chromosome condensation. Chromosoma 108, 412–425.

Costoya, J.A., Hobbs, R.M., Barna, M., Cattoretti, G., Manova, K., Sukhwani, M., Orwig, K.E., Wolgemuth, D.J., Pandolfi, P.P., 2004. Essential role of Plzf in maintenance of spermatogonial stem cells. Nat. Genet. 36, 653–659.

Derry, W.B., Putzke, A.P., Rothman, J.H., 2001. *Caenorhabditis elegans* p53: role in apoptosis, meiosis, and stress resistance. Science 294, 591–595.

Getun, I.V., Wu, Z.K., Khalil, A.M., Bois, P.R., 2010. Nucleosome occupancy landscape and dynamics at mouse recombination hotspots. EMBO Rep. 11, 555–560.

Higa, L.A., Mihaylov, I.S., Banks, D.P., Zheng, J., Zhang, H., 2003. Radiation-mediated proteolysis of CDT1 by CUL4-ROC1 and CSN complexes constitutes a new checkpoint. Nat. Cell Biol. 5, 1008–1015.

Hofmann, J.F., Beach, D., 1994. cdt1 is an essential target of the Cdc10/Sct1 transcription factor: requirement for DNA replication and inhibition of mitosis. EMBO J. 13, 425–434.

Hu, J., McCall, C.M., Ohta, T., Xiong, Y., 2004. Targeted ubiquitination of CDT1 by the DDB1-CUL4A-ROC1 ligase in response to DNA damage. Nat. Cell Biol. 6, 1003–1009.

Kang, M.J., Kim, M.K., Terhune, A., Park, J.K., Kim, Y.H., Koh, G.Y., 1997. Cytoplasmic localization of cyclin D3 in seminiferous tubules during testicular development. Exp. Cell Res. 234, 27–36.

Kim, Y., Kipreos, E.T., 2007. The *Caenorhabditis elegans* replication licensing factor CDT-1 is targeted for degradation by the CUL-4/DDB-1 complex. Mol. Cell. Biol. 27, 1394–1406.

Kim, S.T., Moley, K.H., 2008. Paternal effect on embryo quality in diabetic mice is related to poor sperm quality and associated with decreased glucose transporter expression. Reproduction 136, 313–322.

Kim, J., Feng, H., Kipreos, E.T., 2007. *C. elegans* CUL-4 prevents rereplication by promoting the nuclear export of CDC-6 via a CKI-1-dependent pathway. Curr. Biol. 17, 966–972.

Kneitz, B., Cohen, P.E., Avdievich, E., Zhu, L., Kane, M.F., Hou Jr., H., Kolodner, R.D., Kucherlapati, R., Pollard, J.W., Edelmann, W., 2000. MutS homolog 4 localization to meiotic chromosomes is required for chromosome pairing during meiosis in male and female mice. Genes Dev. 14, 1085–1097.

Kopanja, D., Roy, N., Stoyanova, T., Hess, R.A., Bagchi, S., Raychaudhuri, P., 2011. Cul4A is essential for spermatogenesis and male fertility. Dev. Biol. 352, 278–287.

Lassalle, B., Bastos, H., Louis, J.P., Riou, L., Testart, J., Dutrillaux, B., Fouchet, P., Allemand, I., 2004. 'Side Population' cells in adult mouse testis express Bcrp1 gene and are enriched in spermatogonia and germinal stem cells. Development 131, 479–487.

Liu, L., Lee, S., Zhang, J., Peters, S.B., Hannah, J., Zhang, Y., Yin, Y., Koff, A., Ma, L., Zhou, P., 2009. CUL4A abrogation augments DNA damage response and protection against skin carcinogenesis. Mol. Cell 34, 451–460.

Mahadevaiah, S.K., Turner, J.M., Baudat, F., Rogakou, E.P., de Boer, P., Blanco-Rodriguez, J., Jasin, M., Keeney, S., Bonner, W.M., Burgoyne, P.S., 2001. Recombinational DNA double-strand breaks in mice precede synapsis. Nat. Genet. 27, 271–276.

Moens, P.B., Kolas, N.K., Tarsounas, M., Marcon, E., Cohen, P.E., Spyropoulos, B., 2002. The time course and chromosomal localization of recombination-related proteins at meiosis in the mouse are compatible with models that can resolve the early DNA–DNA interactions without reciprocal recombination. J. Cell Sci. 115, 1611–1622.

Oh, S.D., Lao, J.P., Hwang, P.Y., Taylor, A.F., Smith, G.R., Hunter, N., 2007. BLM ortholog, Sgs1, prevents aberrant crossing-over by suppressing formation of multichromatid joint molecules. Cell 130, 259–272.

Pickart, C.M., 2001. Mechanisms underlying ubiquitination. Annu. Rev. Biochem. 70, 503–533.

Roig, I., Dowdle, J.A., Toth, A., de Rooij, D.G., Jasin, M., Keeney, S., 2010. Mouse TRIP13/PCH2 is required for recombination and normal higher-order chromosome structure during meiosis. PLoS Genet. 6 pii: e1001062.

Russell, L.D., 1990. Histological and Histopathological Evaluation of the Testis. Cache River Press, Clearwater, Fl.

Schiff, J.D., Ramirez, M.L., Bar-Chama, N., 2007. Medical and surgical management male infertility. Endocrinol. Metab. Clin. North Am. 36, 313–331.

Sutovsky, P., 2003. Ubiquitin-dependent proteolysis in mammalian spermatogenesis, fertilization, and sperm quality control: killing three birds with one stone. Microsc. Res. Tech. 61, 88–102.

Svendsen, J.M., Smogorzewska, A., Sowa, M.E., O'Connell, B.C., Gygi, S.P., Elledge, S.J., Harper, J.W., 2009. Mammalian BTBD12/SLX4 assembles a Holliday junction resolvase and is required for DNA repair. Cell 138, 63–77.

Vincent, S., Segretain, D., Nishikawa, S., Nishikawa, S.I., Sage, J., Cuzin, F., Rassoulzadegan, M., 1998. Stage-specific expression of the Kit receptor and its ligand (KL) during male gametogenesis in the mouse: a Kit–KL interaction critical for meiosis. Development 125, 4585–4593.

Vousden, K.H., Lane, D.P., 2007. p53 in health and disease. Nat. Rev. Mol. Cell Biol. 8, 275–283.

Yin, Y., Lin, C., Ma, L., 2006. MSX2 promotes vaginal epithelial differentiation and wolffian duct regression and dampens the vaginal response to diethylstilbestrol. Mol. Endocrinol. 20, 1535–1546.

Zhong, W., Feng, H., Santiago, F.E., Kipreos, E.T., 2003. CUL-4 ubiquitin ligase maintains genome stability by restraining DNA-replication licensing. Nature 423, 885–889.